

Temperature dependence of the thermal boundary resistivity of glass-embedded metal nanoparticles

Francesco Banfi, Vincent Juvé, Damiano Nardi, Stefano Dal Conte, Claudio Giannetti et al.

Citation: *Appl. Phys. Lett.* **100**, 011902 (2012); doi: 10.1063/1.3673559

View online: <http://dx.doi.org/10.1063/1.3673559>

View Table of Contents: <http://apl.aip.org/resource/1/APPLAB/v100/i1>

Published by the [American Institute of Physics](#).

Related Articles

High temperature thermal properties of thin tantalum nitride films

Appl. Phys. Lett. **99**, 261906 (2011)

Ballistic phonon thermal transport in a cylindrical semiconductor nanowire modulated with nanocavity

J. Appl. Phys. **110**, 124321 (2011)

Synthesis of zinc fulleride (ZnxC60) thin films with ultra-low thermal conductivity

J. Appl. Phys. **110**, 124320 (2011)

Interfacial thermal resistance between metallic carbon nanotube and Cu substrate

J. Appl. Phys. **110**, 124314 (2011)

Multiscale modeling of cross-linked epoxy nanocomposites to characterize the effect of particle size on thermal conductivity

J. Appl. Phys. **110**, 124302 (2011)

Additional information on *Appl. Phys. Lett.*

Journal Homepage: <http://apl.aip.org/>

Journal Information: http://apl.aip.org/about/about_the_journal

Top downloads: http://apl.aip.org/features/most_downloaded

Information for Authors: <http://apl.aip.org/authors>

ADVERTISEMENT

**AIP**Advances

Submit Now

**Explore AIP's new
open-access journal**

- **Article-level metrics
now available**
- **Join the conversation!
Rate & comment on articles**

Temperature dependence of the thermal boundary resistivity of glass-embedded metal nanoparticles

Francesco Banfi,^{1,2,a)} Vincent Juvé,^{2,b)} Damiano Nardi,^{1,c)} Stefano Dal Conte,^{3,d)} Claudio Giannetti,¹ Gabriele Ferrini,¹ Natalia Del Fatti,² and Fabrice Vallée²

¹*i-LAMP and Dipartimento di Matematica e Fisica, Università Cattolica, I-25121 Brescia, Italy*

²*FemtoNanoOptics Group, LASIM, Université Lyon 1, CNRS, 69622 Villeurbanne, France*

³*Dipartimento di Fisica A. Volta, Università di Pavia, I-27100 Pavia, Italy*

(Received 26 September 2011; accepted 9 December 2011; published online 3 January 2012)

The temperature dependence of the thermal boundary resistivity is investigated in glass-embedded Ag particles of radius 4.5 nm, in the temperature range from 300 to 70 K, using all-optical time-resolved nanocalorimetry. The present results provide a benchmark for theories aiming at explaining the thermal boundary resistivity at the interface between metal nanoparticles and their environment, a topic of great relevance when tailoring thermal energy delivery from nanoparticles as for applications in nanomedicine and thermal management at the nanoscale. © 2012 American Institute of Physics. [doi:10.1063/1.3673559]

With the ever decreasing size of nanodevices, investigation and modeling of heat exchange at the nanoscale has become of central technological interest. Under a fundamental standpoint, metal nanoparticles (NPs) embedded in a host matrix constitute a model system, as they can be selectively heated-up and their cooling monitored using time-resolved spectroscopy.^{1–3} Furthermore, the thermal dynamics occurring between an optically excited metal nanoparticle and the surrounding environment is of direct relevance for a variety of applications ranging from photothermal cancer therapy^{4,5} and selective drug delivery⁶ to thermoacoustic imaging and electromagnetic waveguiding in dielectric-embedded plasmonic devices.⁷ The electromagnetic energy harvested by the NPs is dissipated as thermal energy in the environment. The corresponding energy flux J_p is ruled by the thermal boundary resistivity ρ_{bd} , i.e., Kapitza resistivity, and by the temperature mismatch ΔT between the two media: $J_p = \Delta T / \rho_{bd}$. Investigating ρ_{bd} is, therefore, crucial to tailor thermal energy delivery from the NP to the matrix or matrix-embedded target and, more generally, to analyze heat transfer at the nanoscale.

Whereas effort has been devoted to understand and model the Kapitza resistivity between two solids, both bulk and thin films,^{8–10} the scenario remains relatively unexplored when one of the two materials downscales to the nanometer range. Several confinement effects may modify ρ_{bd} , for instance, as the dimension of the NPs becomes comparable to the thermal diffusion length of the host material,^{11–13} or is reduced to a point where the continuum solid approximation to the elastic problem becomes questionable. A lack of extensive experimental evidence^{2,14,15} spanning the space of parameters affecting ρ_{bd} , most notably the temperature,^{8,9} has so far prevented a consistent account of the mechanisms

ruling the Kapitza resistivity at the nanoscale. When confronted with the problem of measuring the heat transfer from a nanoscale object, the challenges stand in (a) a probe speed requirement, dictated by the fact that the time for heat exchange between the sample and the thermal reservoir decreases with the decreasing sample's mass and (b) a non-contact probe requirement, to avoid the addendum heat capacitance contribution from the probe itself.

In this letter, we use time-resolved all-optical nanocalorimetry¹⁶ to overcome such challenges and investigate the temperature dependence of the cooling dynamics of glass-embedded Ag particles of radius $R = 4.5$ nm. The Kapitza resistivity is shown to increase by a factor of two with decreasing temperature from 300 to 70 K, a trend consistent with existing models.

The Ag nanospheres are embedded in a 50% BaO–50% P₂O₅ glass matrix of thickness $L = 50$ μ m. The metal volume fraction is $2 \cdot 10^{-4}$. The sample was synthesized using a fusion and heat treatment technique.^{17,18} The samples' optical density (OD) shows enhanced absorption in the blue portion of the spectrum due to the localized surface plasmon resonance (LSPR) of the Ag NPs – see inset of Fig. 1.

The time-resolved measurements were performed using a Ti:Sapphire cavity dumped oscillator – 800 nm wavelength, 120 fs pulse temporal width at full width half maximum. The Ag NPs are selectively excited by the frequency-doubled pulse at 400 nm wavelength close to the LSPR in order to maximize energy absorption in the particle. This leads to a fast heating of the electrons of the NPs that thermalize with the lattice on a few picoseconds time-scale, the thermal energy being subsequently delivered to the matrix. Care was taken to minimize average heating¹⁹ of the glass matrix by keeping the energy per pulse as low as possible while granting a detectable transmission variation. To this end, the laser repetition rate was tuned to 540 kHz by means of a cavity dumper. Accounting for transmission losses along the optical path, the energy density per pump pulse on the sample surface was $I_0 \sim 0.5$ J/m², while the energy density absorbed per particle per pulse was $U_V \sim 4 \cdot 10^7$ J/m³. The cooling dynamics of the hot NPs to the glass matrix is then followed by measuring the

^{a)}Electronic mail: francesco.banfi@dmf.unicatt.it.

^{b)}Present address: Max-Born-Institut für Nichtlineare Optik und Kurzzeitspektroskopie, 12489 Berlin, Germany.

^{c)}Present address: JILA, University of Colorado at Boulder, Boulder, Colorado 80309, USA.

^{d)}Present address: Department of Applied Physics, Eindhoven University of Technology, 5600 MB Eindhoven, The Netherlands.

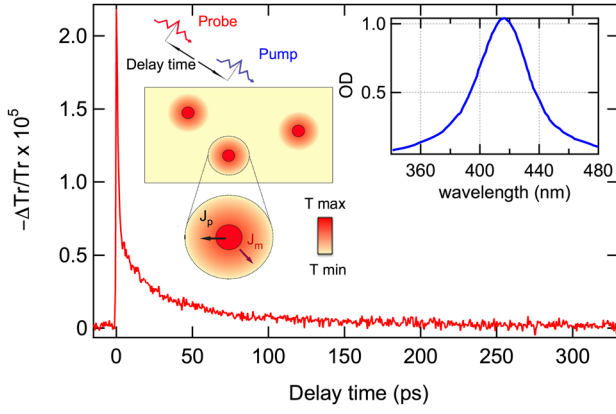


FIG. 1. (Color online) Measured time-resolved relative transmission change for $T_{\text{cryo}}=200$ K. The pump and probe pulses have wavelengths, respectively, at 400 nm and 800 nm. In the cartoon, the thermal fluxes J_p and J_m are represented together with the temperature profile within the sample. Inset: measured OD of the sample outlining the Ag nanoparticles' LSPR.

relative change in transmission across the sample $\Delta\text{Tr}/\text{Tr}$ of a time-delayed 800 nm probe pulse. Probing out of the LSPR grants proportionality between the experimental signal and the NPs temperature rise² (at the expense of the signal amplitude).

A typical experimental trace is reported in Fig. 1 for a cryostat temperature $T_{\text{cryo}}=200$ K. After excitation by the pump pulse and internal electron-lattice thermalization, i.e., after 6 ps (this step has been extensively investigated in these systems^{1,20} and will not be discussed here), the signal decay reflects cooling of the hot NP to the matrix. This is governed by the thermal flux J_p and J_m from the NP to the matrix and from the matrix portion adjacent to the NP to the rest of the matrix, respectively. Considering these two processes, the energy balance is governed by

$$C_p \partial_t T_p(t) = -\frac{3}{R\rho_{bd}} [T_p(t) - T_m(R, t)], \quad (1)$$

$$C_m \partial_t T_m(r, t) = \Lambda_m r^{-1} \partial_r^2 [r T_m(r, t)], \quad (2)$$

where T_p is the NPs temperature, assumed as constant throughout the particle volume, T_m the matrix' temperature, C_p and C_m the particle's and matrix's specific heat per unit volume, respectively, and Λ_m the matrix' thermal conductivity. For the case of *constant* thermal parameters, the temperature increase for the NP, $\Delta T_p(t)$, and for the matrix portion in contact with it, $\Delta T_m(R, t)$, are analytically accessible working in Laplace space²¹ and read

$$\Delta T_p(t) = \int_0^\infty du f(u, t), \quad (3)$$

$$\Delta T_m(R, t) = \int_0^\infty du \left[1 - \frac{u^2}{kgR} \right] f(u, t), \quad (4)$$

where

$$f(u, t) = \frac{2k(Rg)^2 \Delta T_0}{\pi} \frac{u^2 \exp(-\kappa u^2 t / R^2)}{[u^2(1+Rg) - kRg]^2 + (u^3 - kRgu)^2}, \quad (5)$$

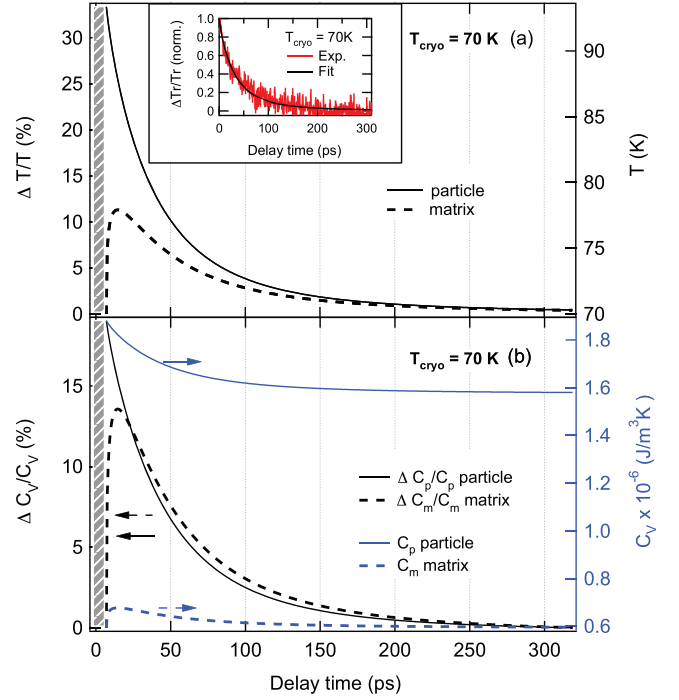


FIG. 2. (Color online) Time evolution of temperature and specific heat for $T_{\text{cryo}}=70$ K. Panel (a): relative temperature variation (left axis) and absolute temperature (right axis) of the NP (full line) and of the adjacent matrix (dashed line). Inset: experimental transmission change normalized to the value at 6 ps (red curve) and its best fit (black curve). Panel (b): relative specific heat variation (left axis) and absolute specific heat (right axis) of the NP (full line) and of the adjacent matrix (dashed line).

where ΔT_0 is the initial temperature increase²² and $\kappa = \Lambda_m / C_m$, $k = 3C_m / C_p$, $g = 1 / \Lambda_m \rho_{bd}$. In our analysis, the thermal resistivity ρ_{bd} is set as a fit parameter, together with Λ_m , which is not precisely known for our glass material.

As low temperatures are investigated (in particular, around and below the NPs Debye temperature, $T_D \sim 215$ K for Ag), C_p and C_m (Ref. 23) cannot be set to their T_{cryo} value and regarded as constant over the particle and matrix's temperature excursion taking place during the experiment. The solution of Eqs. (1) and (2), taking into account the temperature dependent specific heats, is then retrieved iteratively. Fitting is performed starting at a time-delay of 6 ps and setting $T_{m,0} = T_{\text{cryo}}$, and $T_{p,0} = T_{\text{cryo}} + \Delta T_0$. The corresponding values $C_p(T_{p,0})$ and $C_m(T_{m,0})$ are inserted in Eqs. (3) and (4), and the new temperatures $T_{p,1} = T_{\text{cryo}} + \Delta T_{p,1}$ and $T_{m,1} = T_{\text{cryo}} + \Delta T_{m,1}$ are calculated and adopted in the subsequent time step. The procedure is iterated to reach the maximum experimental time-delay of 320 ps. Values for ρ_{bd} and Λ_m are obtained maximizing the likelihood between the theoretical $T_p(t; \rho_{bd}, \Lambda_{bd}) / \Delta T_0$ and experimental $-\Delta\text{Tr}/\text{Tr}$ traces.

The resulting dynamics of temperatures and specific heats is exemplified in Figs. 2(a) and 2(b), respectively, for the lowest studied temperature. The internal thermalization of the NP is achieved at $T_p = 93$ K. As time evolves, the NP cools down, increasing $T_m(R)$; the maximum value of $T_m(R)$ being attained at $t \sim 15$ ps. For longer time-delays, both T_p and $T_m(R)$ decay toward the asymptotic value T_{cryo} . The same trend applies to the specific heats C_p and $C_m(R)$, showing maximum relative changes during the experiment in the 15%-20% range. A similar behavior is obtained for measurements performed at higher

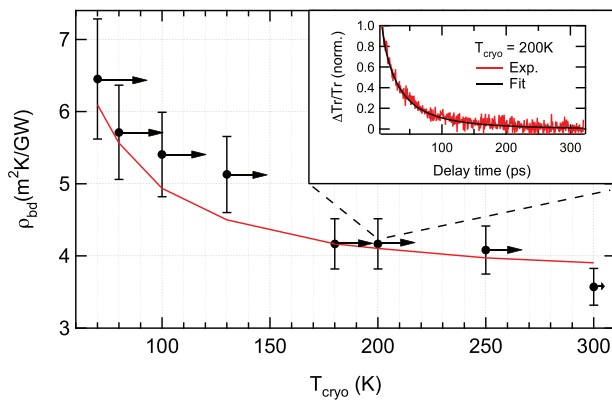


FIG. 3. (Color online) Kapitza resistivity ρ_{bd} vs T_{cryo} (black circles). The horizontal arrows indicate the temperatures spanned by the NPs during the thermalization process. Plot of the function AC_p^{-1} , A being a multiplication constant with dimensions ms^{-1} (red curve). Inset: normalized transmission change (red curve) and its best fit (black curve) for the case $T_{cryo} = 200$ K.

temperatures, although with a smaller excursion amplitude (as indicated by the arrows in Fig. 3). These variations stress the importance of taking into account the temperature dependence of the specific heat when measuring at cryogenic temperatures and make difficult the extraction of ρ_{bd} at values of $T_{cryo} < 70$ K. The Kapitza resistivity $\rho_{bd}(T_{cryo})$ increases by a factor of two, spanning values from 3.2 to 6.5 $\text{m}^2 \text{K/GW}$, as the cryostat's temperature decreases from 300 K to 77 K (see Fig. 3). The extracted value corresponds to a mean value of ρ_{bd} over the NPs temperature excursion during the experiment (indicated by arrows in Fig. 3). Values for Λ_m were found in the range 0.2-0.7 W/mK, comparable to the ones reported for thermal conductivity of glasses with similar compositions.²

Starting from the general expression for the Kapitza resistivity,⁸ and assuming both a frequency independent and/or frequency-averaged phonon transmission coefficient \tilde{t} , and group velocity \tilde{v}_g , one finds $\rho_{bd} \sim (\tilde{t} \tilde{v}_g C_p)^{-1}$. This trend is experimentally retrieved in our data where ρ_{bd} is found to roughly follow the temperature dependence of C_p^{-1} , see Fig. 3.

In conclusion, we measured via time-resolved all-optical nanocalorimetry the Kapitza resistivity of a 4.5 nm radius glass-embedded Ag nanoparticle in the temperature range from 300 K to 70 K. ρ_{bd} increases monotonically from an ambient temperature value of 3.2 $\text{m}^2 \text{K/GW}$ to 6.5 $\text{m}^2 \text{K/GW}$. The present findings constitute a benchmark for theories aiming at explaining the Kapitza resistivity in nanosystems, a fundamental issue for applications in nanomedicine and thermal management at the nanoscale.

We acknowledge Dr. Aurelién Crut and Dr. Paolo Maioli for enlightening discussions and useful suggestions. This work was partially funded by grant D.2.2-2011 of Università Cattolica and the Ophthermal grant of the Agence Nationale de la Recherche. N.D.F. and F.B. acknowledge the support from the Institut Universitaire de France and CNRS, respectively. Open Access publication was sponsored in the frame of Scientific Dissemination Grant D.3.1-2011 of Università Cattolica.

¹G. V. Hartland, *Chem. Rev.* **111**, 3858 (2011).

²V. Juvé, M. Scardamaglia, P. Maioli, A. Crut, S. Merabia, L. Joly, N. Del Fatti, and F. Vallée, *Phys. Rev. B* **80**, 195406 (2009).

³A. Plech, S. Grésillon, G. von Plessen, K. Scheidt, and G. Naylor, *Chem. Phys.* **299**, 183 (2004).

⁴L. R. Hirsch, R. J. Stafford, J. A. Bankson, S. R. Sershen, B. Rivera, R. E. Price, J. D. Hazle, N. J. Halas, and J. L. West, *Proc. Natl. Acad. Sci. U.S.A.* **100**, 13549 (2003).

⁵P. K. Jain, I. H. El-Sayed, and M. A. El-Sayed, *Nanotoday* **2**, 18 (2007).

⁶L. Paasonena, T. Laaksonen, C. Johansb, M. Yliperttula, K. Kontturi, and A. Urttic, *J. Controlled Release* **122**, 86 (2007).

⁷M. Rini, A. Cavalleri, R. W. Schoenlein, R. López, L. C. Feldman, R. F. Haglund, Jr., L. A. Boatner, and T. E. Haynes, *Opt. Lett.* **30**, 558 (2005).

⁸E. D. Swartz and R. O. Pohl, *Rev. Mod. Phys.* **61**, 605 (1989).

⁹R. J. Stoner and H. J. Maris, *Phys. Rev. B* **48**, 16373 (1993).

¹⁰G. Cahill, W. K. Ford, K. E. Goodson, G. D. Mahan, A. Majumdar, H. J. Maris, R. Merlin, and S. R. Phillpot, *J. Appl. Phys.* **93**, 793 (2003).

¹¹M. E. Siemens, Q. Li, R. Yang, K. A. Nelson, E. H. Anderson, M. M. Murnane, and H. C. Kapteyn, *Nature Mater.* **9**, 26 (2010).

¹²G. Chen, *Phys. Rev. Lett.* **86**, 2297 (2001).

¹³M. Rashidi-Huyeh, S. Volz, and B. Palpant, *Phys. Rev. B* **78**, 125408 (2008).

¹⁴A. Plech, V. Kotaidis, S. Grésillon, C. Dahmen, and G. von Plessen, *Phys. Rev. B* **70**, 195423 (2004).

¹⁵O. M. Wilson, X. Hu, D. G. Cahill, and P. V. Braun, *Phys. Rev. B* **66**, 224301 (2002).

¹⁶F. Banfi, F. Pressacco, B. Revaz, C. Giannetti, D. Nardi, G. Ferrini, and F. Parmigiani, *Phys. Rev. B* **81**, 155426 (2010).

¹⁷K. Uchida, S. Kaneko, S. Omi, C. Hata, H. Tanji, Y. Asahara, A. J. Ikushima, T. Tokizaki, and A. Nakamura, *J. Opt. Soc. Am. B* **11**, 1236 (1994).

¹⁸A. Nelet, A. Crut, A. Arbouet, N. Del Fatti, F. Vallée, H. Portales, L. Saviot, and E. Duval, *Appl. Surf. Sci.* **229**, 226 (2004).

¹⁹C. Giannetti, B. Revaz, F. Banfi, M. Montagnese, G. Ferrini, F. Cilento, S. Maccalli, P. Vavassori, G. Oliviero, E. Bontempi *et al.*, *Phys. Rev. B* **76**, 125413 (2007).

²⁰A. Arbouet, C. Voisin, D. Christofilos, P. Langot, N. Del Fatti, F. Vallée, J. Lermé, G. Celep, E. Cottancin, M. Gaudry *et al.*, *Phys. Rev. Lett.* **90**, 177401 (2003).

²¹H. S. Carslaw and J. C. Jaeger, *Conduction of Heat in Solids* (Oxford University Press, Oxford, 1959).

²²The value ΔT_0 is evaluated solving $U_V = \int_{T_{cryo}}^{T_{cryo} + \Delta T_0} C_p(T) dT$, the electrons' contribution to the specific heat being negligible for the explored temperature range.

²³ $C_m(T)$ was taken from SciGlass data base, $C_p(T)$ from F. Meads, W. R. Forsythe, and W. F. Giauque, *J. Am. Chem. Soc.* **63**, 1902 (1941).